Cloud Publications
International Journal of Advanced Remote Sensing and GIS
2016, Volume 5, Issue 9, pp. 1896-1907
ISSN 2320 - 0243, Crossref: 10.23953/cloud.ijarsg.68

Research Article | Open Access

Characterization of Potential Springs in the Lower Colorado Desert of Southern California using Satellite Radar and Landsat Time Series Analysis

Christopher Potter

Senior Scientist, NASA Ames Research Center, United States

Publication Date: 13 September 2016

DOI: https://doi.org/10.23953/cloud.ijarsg.68

Abstract Renewable energy development in southern California is receiving increasing attention due to potential impacts on wildlife habitats and water sources. This study was designed to quantify and map, for the first time, sub-surface water sources from springs in the Lower Colorado Desert area of southern California using satellite radar data and 30 years of Landsat satellite image data. Synthetic Aperture Radar (SAR) data was used to identify sub-surface water sources not already documented as springs or seeps in the National Hydrography Database. Landsat imagery starting in 1985 was used to characterize vegetation growth patterns at these suspected spring locations detected from SAR analysis. Results showed a total of 104 potential spring locations across the Lower Colorado Desert study area, 19 of which were detected within Solar Energy Zone (SEZ) development boundaries, roughly evenly split between Riverside East and Imperial East, and 13 of which (both inside and outside SEZs) showed relatively high green vegetation index values over the period of 1985 to 2015 that would depend on non-precipitation water sources associated with active springs.
Keywords *Radar; Landsat; Surface Water; Springs; Seeps; Solar Energy Development; Lower Colorado Desert; DRECP*

1. Introduction

Under the surface of the Mojave and Sonoran-Colorado Deserts of California is a complex system of groundwater stored in underground aquifer layers of fractured rock. The depth at which an aquifer becomes saturated is called the water table. A natural spring or seep occurs where the water table exceeds or breaches the soil surface from underneath. In general, if water from beneath the surface is regularly observed flowing upwards from a well-defined source, then it is called a spring. If it simply forms a constantly wet, ponded area on the surface from a poorly defined sub-surface source, then it is called a seep. Spring areas usually include the orifice area and out-flow stream or springbrook (Patten et al., 2007).

Springs and seeps in the southern California deserts support numerous sensitive and threatened plant and animal species (Randall et al., 2010). Human activities over the last 100 years, such as

groundwater pumping for agricultural irrigation and mining developments, have destroyed or profoundly altered many of these rare wetland habitats (Patten et al., 2007; USFWS, 2009).

Renewable energy in newly proposed Development Focus Areas (DFAs) of southern California is receiving increasing attention due to potential impacts on wildlife habitats and water sources. To mitigate and monitor the impacts of solar facility construction projects, the Desert Renewable Energy Conservation Plan (DRECP, 2016) has become a major component of the State of California Renewables Portfolio Standard. The DRECP provides effective environmental protections and natural resource conservation of desert ecosystems as appropriate development of renewable energy projects advances in southern California.

The DRECP covers parts of seven California counties: Imperial, Inyo, Kern, Los Angeles, Riverside, San Bernardino, and San Diego. Approximately 91,000 km^2 of federal and non-federal California desert land are part of the DRECP Area. By the end of 2016, the Final DRECP Record of Decision (ROD) will be completed for BLM public lands under agency jurisdictions within the DRECP area.

The objective of this remote sensing data analysis for southern California deserts was to quantify and characterize, for the first time, sub-surface water sources and potential springs in the Lower Colorado Desert area using satellite L-band Synthetic Aperture Radar (SAR) data together with 30 years of Landsat satellite reflectance data. Satellite SAR data were used to identify sub-surface water sources not already documented as springs or seeps in the National Hydrography Database (NHD; USGS, 1999), whereas Landsat imagery starting in 1985 was used to characterize vegetation growth patterns at these suspected spring locations detected from SAR analysis. The normalized difference vegetation index (NDVI) from Landsat has been closely correlated with percent cover measurements of green vegetation canopies in arid ecosystems, as reported in numerous published studies (Anderson et al., 1993; Elmore et al., 2000; Huang et al., 2010).

2. Study Area

The area of interest for this Landsat data study within the southern DRECP region was the Lower Colorado Desert of California (Figure 1). This area is bounded on the west by the Laguna, Santa Rosa, and San Jacinto mountain ranges, on the east by the California-Arizona state line, on the north by the gradual transition to the Mojave Desert, and on the south by the California-Mexico border (Marks, 1950). Low annual rainfall (50 – 300 mm) and high average daily temperatures (reaching 45^{o}C in the summer) make this area one of the most arid in North America. Vegetation communities in the Colorado Desert have been classified into seven basic types: creosote bush scrub, cactus scrub, saltbush scrub, alkali sink, microphyll woodland, psammaophytic scrub, and palm oasis (Schoenherr and Burk, 2007).

The National Hydrography Database (USGS, 1999) includes 548 known spring features in the Lower Colorado Desert study area. The majority of these known springs in the NHD are located in eastern San Diego County. Only five of the known springs in the NHD are located in renewable energy DFA zones of the Lower Colorado Desert.

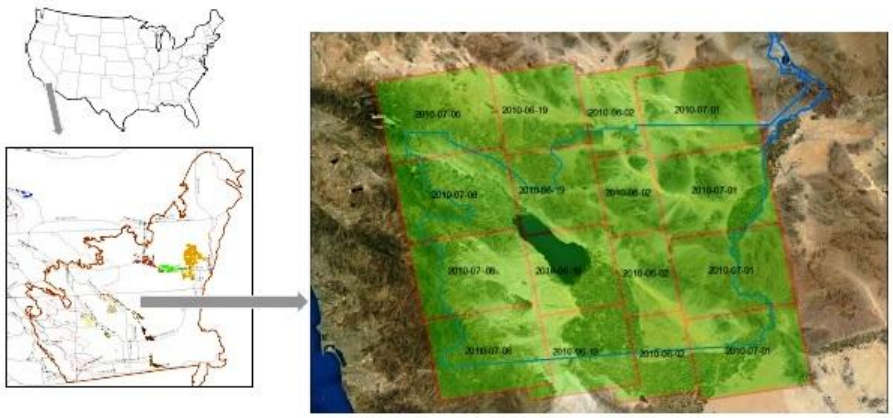

Figure 1: *Lower Colorado Desert study area with the footprint of PALSAR images acquired in FBD mode*

3. Methods

3.1. Sub-Surface Water Anomaly Detection from SAR

Spaceborne L-band SAR data from the Advanced Land Observing Satellite/Phased Array (ALOS/PALSAR) sensor was acquired for the Lower Colorado Desert study area. PALSAR data sets were acquired from the Japan Aerospace Exploration Agency (JAXA) with Fine Beam Single polarization (FBS, look angle 34.3˚, HH-polarization, and a 6.25m×6.25m ground resolution) with Fine Beam Double Polarization (FBD, look angle 34.3˚, HH- and HV-polarization, ground resolution approximately 12.5m×12.5m). In FBS mode, ALOS/PALSAR can be operated with either HH- or VV-polarization with a bandwidth of 28 MHz. In FBD mode, the polarization options are HH/HV or VV/VH at 14-MHz bandwidth. FBS polarization (HH or VV) and FBD polarization (HH+HV or VV+VH) of PALSAR data have a look angle varying between 7° and 51° (8-60° incidence angle). The operating sensor frequency is 1.27GHZ, which corresponds to a wavelength of 23.6 cm (L-band). L-band images from PALSAR were acquired for June/July 2010 (12.5m, HH and HV polarization) coinciding with dry season, and for November/December 2010 (12.5m, HH and HV polarization) coinciding with wet season (as listed in Table 1 and Figure 1).

Table 1: *Listing of PALSAR imagery datasets acquired for sub-surface soil water detection*

ID	Name	Observation Mode	Polarization	Capture Date
1	ALPSRP231960640	FBD	HH/HV	2010-06-02
2	ALPSRP231960650	FBD	HH/HV	2010-06-02
3	ALPSRP231960660	FBD	HH/HV	2010-06-02
4	ALPSRP231960670	FBD	HH/HV	2010-06-02
5	ALPSRP234440640	FBD	HH/HV	2010-06-19
6	ALPSRP234440650	FBD	HH/HV	2010-06-19
7	ALPSRP234440660	FBD	HH/HV	2010-06-19
8	ALPSRP234440670	FBD	HH/HV	2010-06-19
9	ALPSRP236190640	FBD	HH/HV	2010-07-01

10	ALPSRP236190650	FBD	HH/HV	2010-07-01
11	ALPSRP236190660	FBD	HH/HV	2010-07-01
12	ALPSRP236190670	FBD	HH/HV	2010-07-01
13	ALPSRP236920640	FBD	HH/HV	2010-07-06
14	ALPSRP236920650	FBD	HH/HV	2010-07-06
15	ALPSRP236920660	FBD	HH/HV	2010-07-06
16	ALPSRP236920670	FBD	HH/HV	2010-07-06
17	ALPSRP254570640	FBD	HH/HV	2010-11-04
18	ALPSRP254570650	FBD	HH/HV	2010-11-04
19	ALPSRP254570660	FBD	HH/HV	2010-11-04
20	ALPSRP254570670	FBD	HH/HV	2010-11-04
21	ALPSRP257050640	FBD	HH/HV	2010-11-21
22	ALPSRP257050650	FBD	HH/HV	2010-11-21
23	ALPSRP257050660	FBD	HH/HV	2010-11-21
24	ALPSRP257050670	FBD	HH/HV	2010-11-21
25	ALPSRP258800640	FBD	HH/HV	2010-12-03
26	ALPSRP258800650	FBD	HH/HV	2010-12-03
27	ALPSRP258800660	FBD	HH/HV	2010-12-03
28	ALPSRP258800670	FBD	HH/HV	2010-12-03

The Alaska Satellite Facility (ASF) provided range compression using Fast Fourier Transform (FFT), secondary range compression using range migration compensation, range migration curvature corrections, azimuth compression, multi-look processing and performed conversion from slant to ground range (PALSAR User's Guide, 1st edition, March 2006). MapReady software version 3.1.22 (*http://www.asf.alaska.edu/downloads/software_tools*), developed by ASF, was used to process ALOS/PALSAR imagery, following the methodology steps from Li and Potter (2012):

Step 1: ***Radiometric Calibration*** Calibrating a SAR image involves the process of converting a linear amplitude image into a radiometrically calibrated power image. The input image starts in units of digital numbers (DNs), where the output image is in units of β°, γ°, or σ°. Backscatter is the portion of the outgoing radar signal that the target redirects directly back towards the radar antenna. It is a measure of the reflective strength of a radar target. The normalized measure of the radar return from a distributed target is called the backscatter coefficient, σ°, or sigma naught, and is defined per unit area on the ground. An undesired signal formed by backscatter is called clutter. Other portions of incident radar energy may be reflected and scattered away from the radar or absorbed.

The radar backscatter coefficient (σ°) is the ratio of the power that reflected from a patch of ground in relation to the power sent to the patch of ground, and serves as a quantitative reference measure to the ground. The coefficient can be retrieved from SAR images by using the following equation:

$$\sigma^{\circ} = a_2 (DN^2 - a_1 Nr)$$

where DN = the digital number of the original pixel value

Nr = the noise offset as a function of range
a_1 = the noise scale factor determined during processor calibration
a_2 = a linear conversion factor determined during processor calibration.

The σ˚ value resulting from the equation above is in a power scale. Conversion of these values into decibel (dB) values followed the relationship:

dB = 10 * log_{10} (power scale)

Step 2: ***Terrain Correction*** SAR images are acquired with side-looking geometry. This format leads to a number of distortions in the imagery: foreshortening, layover, and shadow (Figure 2). Terrain correction removes these geometry-induced distortions by using a digital elevation (DEM). The process of terrain correction includes geometric terrain correction and radiometric terrain correction. Geometric terrain correction adjusts the individual pixels of an amplitude image to be in their proper locations. Radiometric terrain correction adjusts the brightness of the pixels with respect to the observation geometry, defined by the incidence angle as well as the slope and aspect of the local terrain.

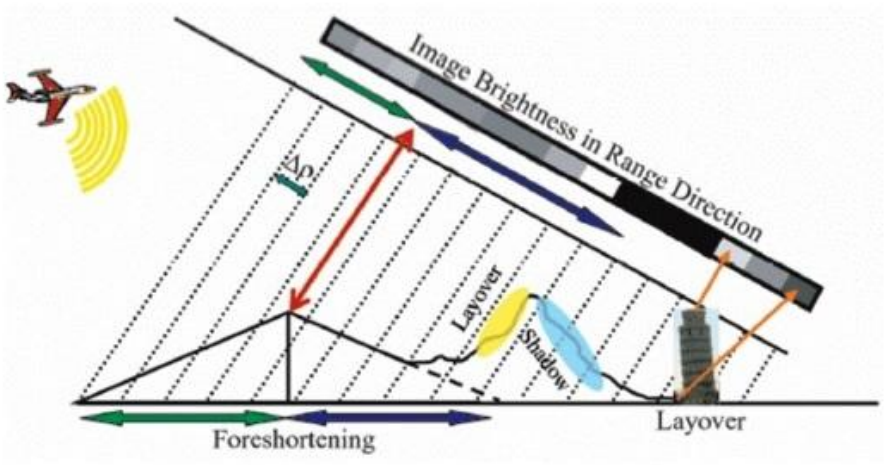

Figure 2: *Schematic of terrain with foreshortening, layover, and shadow effects experienced in SAR image processing (from Li and Potter, 2012)*

Step 3: ***Geocoding*** The geocoding step is essential to correlate the SAR image geometry to the actual terrain. By transforming the image from SAR geometry into one of the standard map projections, the SAR image can be imported into imager processing applications for further analysis. The geocoding step is invoked by turning on the “Geocode” module from MapReady with a UTM projection. For the PALSAR scene of the I-10 corridor, the parameters for UTM zone 11N and the WGS84 datum were used. As part of the transformation from SAR geometry into map-projected space, a bi-linear method was used to resample the data values. Compared to nearest-neighbor and bi-cubic approaches, the bi-linear interpolation scheme considers four neighboring pixel values.

Step 4: ***Speckle Filtering*** SAR images were filtered to reduce the effect of speckle by utilizing a Kuan filter with a 3×3 kernel. The resultant imagery preserved the mean values, while decreasing the standard deviation of homogeneous targets, and visually preserving the feature edges.

A threshold value (greater than -15 dB) of the preprocessed radar backscatter signals was set to detect pixels with sub-surface water anomalies across the study area. Single or scattered pixels were removed in the newly created sub-surface water anomaly layer. Only clustered pixels were retained for

further “hot spot” analysis. Using visual inspection, pixel clusters with known ground features (i.e. high radar backscatter coefficient caused by terrain relief, transmission towers, communication towers, single buildings, major roadways and river courses, developed residential areas, croplands, and known springs in the NHD) were eliminated from the water anomaly layer. All the suspected sub-surface water sources on slopes less than 10% were converted into potential spring point features for further historical evaluation with Landsat green vegetation index records, mainly to exclude rugged mountainous areas where future renewable energy development activities would not likely take place (Kwartin et al., 2012).

3.2. Landsat Imagery

For this study, near cloud-free imagery from the Landsat sensor was selected from the United States Geological Survey (USGS) Earth Explorer data portal (available online at earthexplorer.usgs.gov) for the years 1985 to 2015. Landsat scenes from path/row 39/37 were acquired during the period of April - May of each year, just following the peak flowering period in the Lower Colorado Desert growing season (Schoenherr and Burk, 2007). All images used in this study were geometrically registered (UTM Zone 11) using terrain correction algorithms (Level 1T) applied by the USGS EROS Data Center.

For the Landsat 4-5 Thematic Mapper (TM) images acquired between 1985 and 2011, 30-m resolution surface reflectance data were generated from the Landsat Ecosystem Disturbance Adaptive Processing System (Masek et al., 2006). Moderate Resolution Imaging Spectroradiometer (MODIS) atmospheric correction routines were applied to Level-1 TM data products. Water vapor, ozone, geopotential height, aerosol optical thickness, and digital elevation are input with Landsat data to the Second Simulation of a Satellite Signal in the Solar Spectrum (6S) radiative transfer models to generate top of atmosphere (TOA) reflectance, surface reflectance, brightness temperature, and masks for clouds, cloud shadows, adjacent clouds, land, snow, ice, and water. Landsat 8 (after 2012) surface reflectance products were generated from the L8SR algorithm, a method that uses the scene center for the sun angle calculation and then hard-codes the view zenith angle to 0. The solar zenith and view zenith angles are used for calculations as part of the atmospheric correction.

4. Results and Discussion

A total of 104 potential spring locations were identified from the 2010 PALSAR image analysis across the Lower Colorado Desert study area (Figure 3). There were 19 potential springs located within DFA boundaries, roughly evenly split between Riverside East and Imperial East Solar Energy Zones (SEZs).

Outside of the DFA zones, 10 potential spring locations were clustered along the Interstate Highway 10 in Riverside County, and about 15 other potential springs were located north of the Riverside East SEZ. Another 10 potential spring locations were clustered in western Imperial County, outside of any DFA zone.

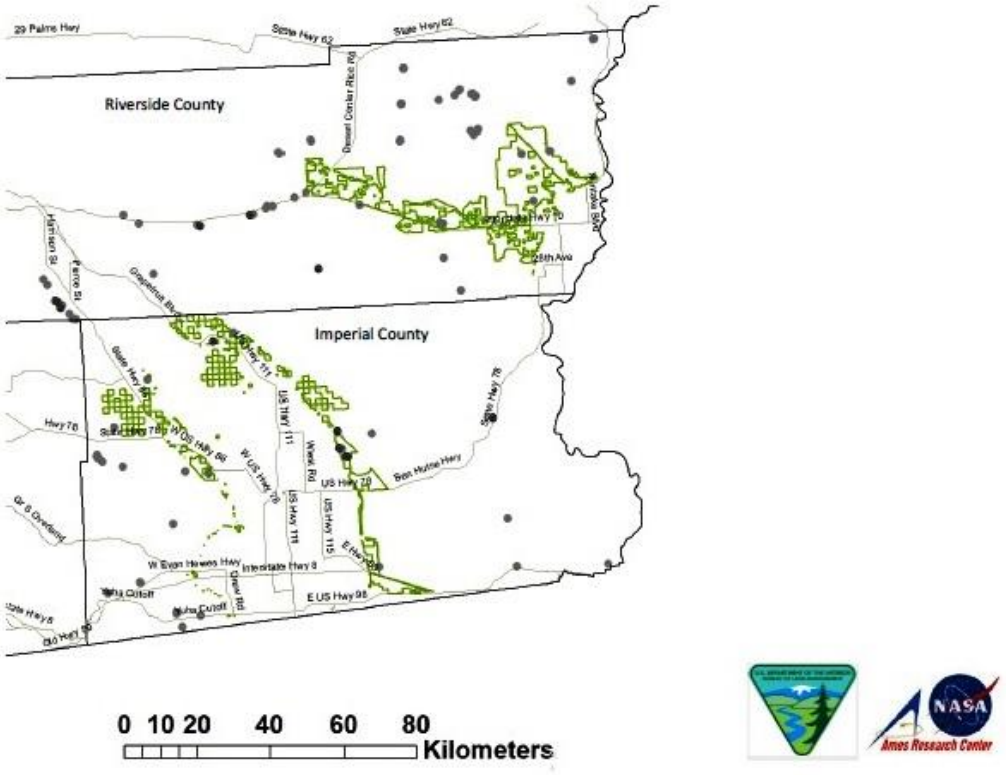

Figure 3: *Potential spring locations (gray points) from 2010 PALSAR image analysis across the Lower Colorado Desert study area. Point labels with a dot in the center were those potential springs detected with Landsat green vegetation index values in excess of 2000 NDVI units during the period of 1985 to 2015. Solar energy zones (SEZ) DFAs were outlined in green*

Landsat NDVI time series data extracted for all 104 potential springs locations showed that only 13 (Figure 3) had green vegetation index values in excess of 2000 NDVI units during the period of 1985 to 2015. Potter (2016) reported that Landsat vegetation index values for desert shrub vegetation averaged across Lower Colorado study area never exceeded 2000 NDVI units, even during the relatively wet precipitation years of 1995, 1998, 2005, and 2010. In contrast, vegetation cover averaged from developed residential zones within the study did regularly exceed 2000 NDVI units, presumably due to urban irrigation practices, except during the driest precipitation years of 2000, 2003, 2007, and 2013-14. This baseline of 2000 NDVI units was therefore established as the indicator level for periodic vegetation growth that would depend on non-precipitation, sub-surface water sources associated with active springs.

A closer examination of potential spring locations where the green vegetation index values periodically exceeded 2000 NDVI units showed highest green cover periods were consistently detected in the years 1992, 2005 and 2010 (Figure 4). The three locations detected in Riverside County were within the Barton Canyon drainage (Seaber et al., 1987) south of Palm Desert (Figure 4a), within the Maniobra Valley drainage south of Interstate Hwy 10 (Figure 4b), and within the Gulliday Well drainage (Figure 4c), for a total of five potential springs all outside of DFA zones.

One potential spring detected above the baseline of 2000 NDVI units in Imperial County (located north of Niland Marina, Figure 4d) was within a DFA zone and showed a different NDVI time series pattern from all the others. In this area, vegetation greenness levels remained below 1000 NDVI units until 2010, after which the green cover increased rapidly to NDVI values in excess of 4000 units by 2015. The true-color image of the areas in Figure 4d indicated that this sub-surface moisture source may

have resulted from a new flow pathway of water into the Salton Sea just to south of this potential spring location.

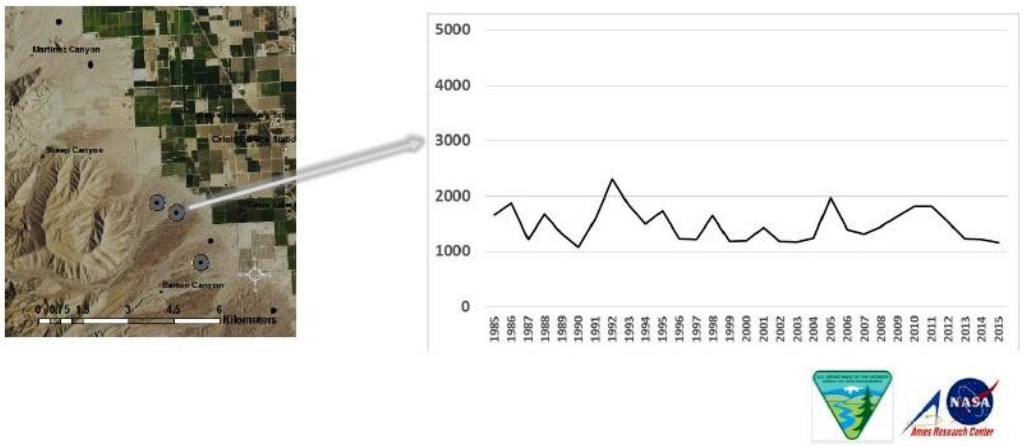

4a: Martinez Canyon to Barton Canyon south of Palm Desert, Riverside County (33.4731N, -116.1505 W)

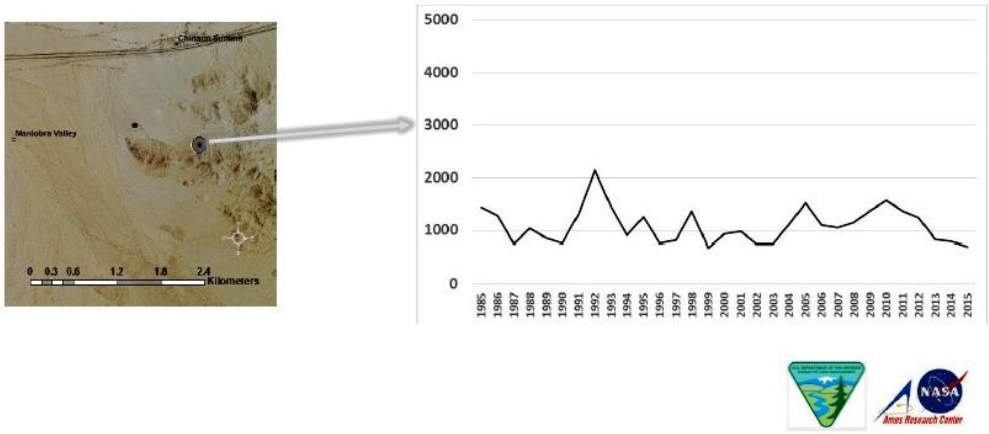

4b: Maniobra Valley south of Hwy 10, Riverside County (33.6133 N, -115.6769 W)

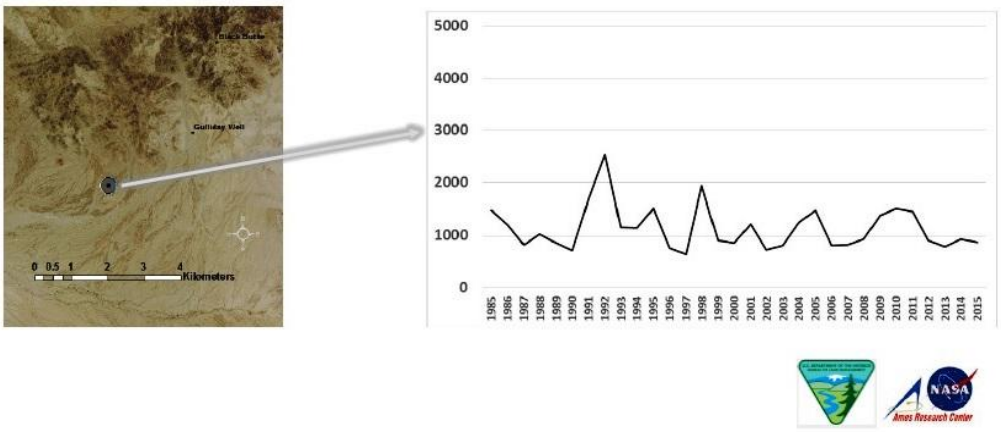

4c: Near Gulliday Well, southern Riverside County (33.4910 N, -115.3012 W)

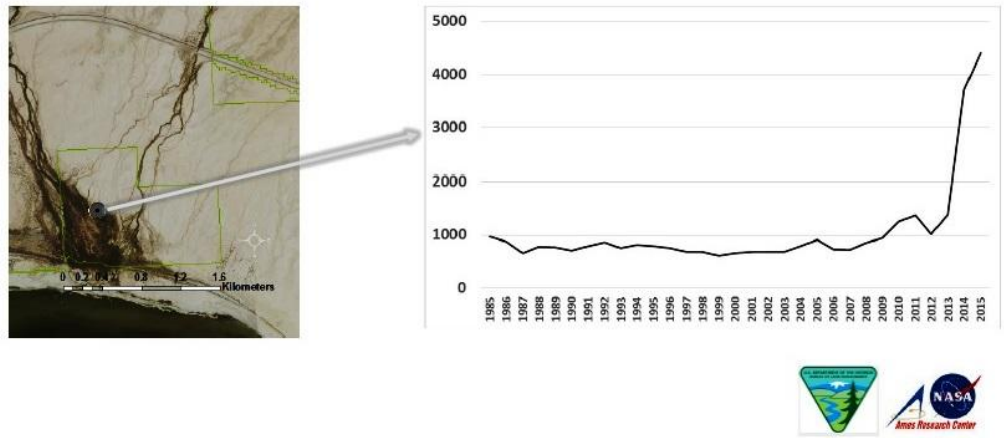

4d: North of Niland Marina DFA, Imperial County (33.3599 N, -115.6954 W)

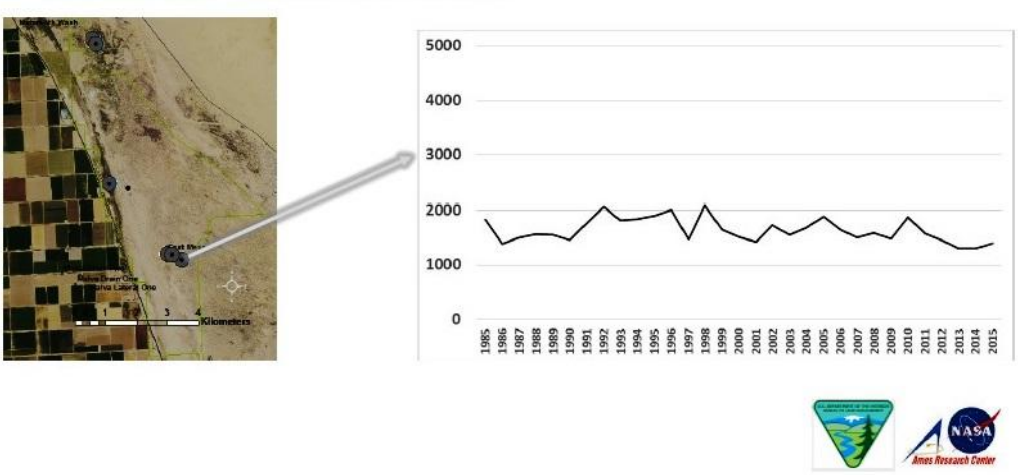

4e: East Mesa DFA, Imperial County (33.008 N, -115.2609 W)

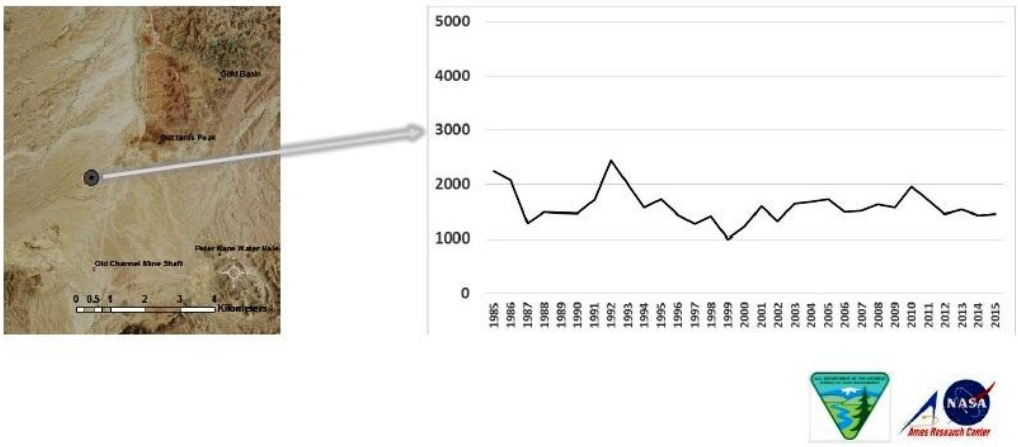

4f: Peter Kane Water Hole near State Hwy 78, Imperial County (33.1349 N, -114.8869 W)

Figure 4: *Time series plots for Landsat NDVI for the years 1985 to 2015 from the months of April–May for potential spring locations where the green vegetation index values periodically exceeded 2000 NDVI units. True color satellite image of the potential spring area and location markers (as in Figure 3) detected from PALSAR data analysis*

The other two potential spring areas detected above the baseline of 2000 NDVI units in Imperial County were located in the East Mesa DFA zone (Figure 4e), and another potential spring farther to the east in the Midway Well drainage (Seaber et al., 1987) near State Hwy 78 (Figure 4f) outside of any DFA zone. Both of these locations showed highest green cover periods detected in the years 1992 and 2010.

The remaining 91 potential spring locations that did not show greenness levels above the baseline of 2000 NDVI units over the period 1985 to 2015 appeared to have vegetation cover patterns similar to the barren dune areas reported by Potter (2016) in the Lower Colorado Desert study area. In general, the yearly greenness levels for most of these potential spring locations remained at or below 1000 NDVI units. It is plausible that analysis of 2010 PALSAR images detected residual sub-surface moisture or ponded surface water in seep-like features at these locations, despite there being insufficient water from below the soil surface to support more than the growth of sparse desert shrub cover nearby.

It is plausible that some seep-like, largely unvegetated ponds detected using PALSAR image data in the Lower Colorado Desert actually corresponded to summer breeding habitats for amphibian species such as Couch's Spadefoot (*Scaphiopus* couchi) and Western Spadefoot (*Spea hammondii*). Spadefoots remain burrowed underground for most of the year and remain under-ground for consecutive years, but appear at the soil surface after the first heavy summer precipitation event to breed in temporary rain-fed ponds on the same night as the event occurs (Mayhew, 1965). Reports of this type of amphibian breeding habitat have been made in areas east of the Algodones Dunes and along State Hwy 78 (Dimmitt and Ruibal, 1980).

5. Conclusions

Satellite radar data sets were shown to successfully detect sub-surface water locations in the Lower Colorado Desert where Landsat NDVI was also measured at levels of vegetation growth that would depend on non-precipitation water sources associated with active springs.

None of the total 104 potential spring locations identified from PALSAR image analysis across the study area were previously listed in the National Hydrography Database (USGS, 1999).

A high priority for field-based verification of spring locations should be given to the 19 potential springs located within solar energy DFA boundaries.

In any case, solar energy project developers can benefit from the satellite image mapping of locations of potential springs and seeps in advance, so that the design of project footprints excludes these rare desert habitats for plants and animals at the start.

Acknowledgements

PALSAR image processing and application of mathematical algorithms for sub-surface water mapping was carried out primarily by Shuang Li of California State University Monterey Bay. This research was supported by funding from the BLM California State Office, Sacramento, CA.

References

Anderson, G.L., Hanson, J.D., and Haas, R.H. Evaluating Landsat Thematic Mapper Derived Vegetation Indices for Estimating above Ground Biomass on Semiarid Rangelands. *Remote Sensing of Environment.* 1993. 45; 165-175.

Cooke, R.U., and Warren, A., 1973: *Geomorphology in Deserts*. London: B.T. Batsford Ltd. 120.

Dimmitt, M.A., and Ruibal, R. Environmental Correlates of Emergence in Spadefoot Toads (*Scaphiopus*). *J. Herpetol.* 1980. 14; 21-29.

DRECP, 2010: Recommendations of Independent Science Advisors for The California Desert Renewable Energy Conservation Plan (DRECP) prepared for Renewable Energy Action Team.

Elmore, A.J., Mustard, J.F., Manning, S.J., and Lobell, D.B. Quantifying Vegetation Change in Semiarid Environments: Precision and Accuracy of Spectral Mixture Analysis and the Normalized Difference Vegetation Index. *Remote Sensing of Environment*. 2000. 73; 87-102.

Huang, S., Potter, C., Crabtree, R.L., Hager, S., and Gross, P. Fusing Optical and Radar Data to Estimate Sagebrush, Herbaceous, and Bare Ground Cover in Yellowstone. *Remote Sensing of Environment.* 2010. 114; 251-264.

Lentile, L., Holden, A., Smith, A., Falkowski, M., Hudak, A., Morgan, P., et al. Remote Sensing Techniques to Assess Active Fire Characteristics and Post-Fire Effects. *International Journal of Wildland Fire.* 2006. 15; 319-345.

Li, S., and Potter, C.S. Patterns of Aboveground Biomass Regeneration in Post-Fire Coastal Scrub Communities. *GIScience & Remote Sensing*. 2012. 49; 182-201.

Kwartin, R., Alexander, S., Anderson, M., Clark, D., Collins, J., Lamson, C., Martin, G., Mayfield, R., McAlpine, L., Moreno, D., Patterson, J., Schultz, C., and Stiever, E. Solar Energy Development on Department of Defense Installations in the Mojave and Colorado Deserts, ICF International, San Jose, California, January 2012. 140.

Marks, J.B. Vegetation and Soil Relations in the Lower Colorado Desert. *Ecology*. 1950. 31; 176-193.

Masek, J.G., Vermote, E.F., Saleous, N., Wolfe, R., Hall, F.G., Huemmrich, F., Gao, F., Kutler, J., and Lim, T.K. A Landsat Surface Reflectance Data Set for North America, 1990-2000. *Geo-science and Remote Sensing Letters.* 2006. 3; 68-72.

Mayhew, W.W. Adaptations of the Amphibian, Scaphiopus Couchii to Desert Conditions. *Am. Midl. Nat.* 1965. 74; 95-109.

Patten, D.T., Rouse, L., and Stromberg, J.C. Isolated Spring Wetlands in the Great Basin and Mojave Deserts, USA: Potential Response of Vegetation to Groundwater Withdrawal. *Environmental Management.* 2008. 41 (3) 398-413.

Potter, C. Landsat Time Series Analysis of Vegetation Changes in Solar Energy Development Areas of the Lower Colorado Desert, Southern California. *Journal of Geoscience and Environment Protection*. 2016. 4; 1-6.

Randall, J.M., Parker, S.S., Moore, J., Cohen, B., Crane, L., Christian, B., Cameron, D., MacKenzie, J., Klausmeyer, K., and Morrison, S., 2010: Mojave Desert Ecoregional Assessment. Unpublished Report. The Nature Conservancy, San Francisco, CA. 106.

Schoenherr, A.A., and Burk, J.H., 2007: *Colorado Desert Vegetation*. Pages 657-682 in Barbour, M.G., Keeler-Wolf, T., and Schoenherr, A.A. (Eds.), *Terrestrial Vegetation of California*, 3rd ed. University of California Press, Berkeley, California. 712.

Seaber, P.R., Kapinos, F.P., and Knapp, G.L., 1987: Hydrologic Unit Maps: U.S. Geological Survey Water-Supply Paper 2294. 63.

U.S. Fish and Wildlife Service (USFWS), 2009: Desert National Wildlife Refuge Complex Ash Meadows, Desert, Moapa Valley, and Pahranagat National Wildlife Refuges, Final Comprehensive Conservation Plan and Environmental Impact Statement Summary, Sacramento, CA. 42.

U.S. Geological Survey (USGS), 1999: Standards for National Hydrography Dataset, Reston, VA.